Chapter 3

Bolted Joint Diagnostics

3.1 Introduction

Components of mechanical systems are often assembled at joints held together by bolts. Unfortunately, bolted joints are subject to a variety of common modes of failure. These include self-loosening, shaking apart, breaking, breaking because of corrosion, stress cracking or fatigue, slippage, which can change the way a structure absorbs load, leakage of corrosive substances in the joint and separation leading to rapid fatigue (Lovell and Pines 1998). The self-healing joint concept addresses the self-loosening mode of failure. However, in order to develop the self-sensing and self-healing joint concept, it is necessary to be able to identify when to actuate the preload restoring washer. For this an understanding of the dynamics of bolted joints is needed.

3.2 Literature Review

A great deal of research has been focused on examining the dynamics of bolted joints, however, their behavior is still not completely understood since it is often nonlinear. One of the most important characteristics of bolted joints is their capacity for damping as a result of friction between the members of the joints. Extensive reviews of this subject by Esteban (1996) and Gaul and Nitsche (2001) have been completed. Beards and Williams (1977) classify the frictional damping as macro-slip, occurring at low clamping pressures, micro-slip, occurring at increasing bolt pressure with very small displacements, or plastic-deformation, occurring at extremely high clamping pressure causing plastic deformations of the roughness.

Many models of the friction mechanisms in joints have been developed. The simplest models relate the force of friction to the relative velocities of sliding surfaces. These include the Coulomb's law, the Elasto Slip Models such as Coulomb's law with a threshold force, referred to as a Jenkins or Masing Element, and Stribeck's model incorporating a decreasing then increasing force with velocity (Gaul 2001).

Friction can not always be described only as a function of velocity. Examples include the Valanis model (Valanis 1971) and LuGre model. Based on a dynamic friction model by Dahl (1976), the LuGre model represents contact surface irregularities as bristles that deflect like springs when a tangential force is applied (Canudas de Wit et al. 1995). A form of this model is considered later.

Since loosening is a pervasive problem with bolted joints, several studies have focused specifically on monitoring bolted joints. Lovell and Pines (1998) developed a wave propagation approach capable of detecting a loss of preload in civil structure joints. Esteban (1996) investigates many issues of using the impedance method with bolted joints. Linear and nonlinear analytical models of a one-dimensional bolted structure were developed. These were then used to examine issues of the impedance method such as attenuation across a joint, the effect of surface treatments in a joint and the effect of variations in bolt tension.

3.3 Investigation of Natural Frequency Variations with Changes in Torque

An investigation of natural frequency variation using both the impedance method and traditional modal analysis methods was performed. The bolted joint used in the experiments described in the second chapter was used.

3.3.1 Modal Experiment

The beam was excited with a random signal from a SigLab analyzer from 0 to 5000 Hz using one of the PZT's closest to the bolt (PZT three in diagram). The remaining PZT's acted as strain sensors from which the frequency response functions (FRF's) were measured. This was done with the bolt tightened to five torque loadings (hand-tightened, 10 ft-lb, 20 ft-lb, 30 ft-lbs and 40 ft-lbs). The torque wrench used to measure bolt torque is incremented in 25 in-lbs and has a range of +/– 600 in-lbs. Figure 3.1 shows the magnitude of the FRFs for PZT four at each torque level.

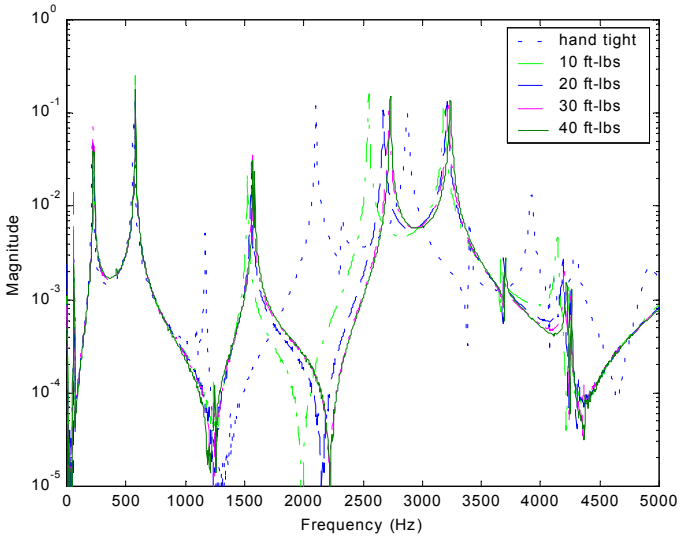

Figure 3.1 Magnitude of FRF for varying torques

3.3.2 Impedance Experiment

After each set of FRF data was taken, impedance measurements were made using the HP4194A Impedance Analyzer. Typically impedance measurements are made at frequencies greater than 30 kHz, however, in order to be able to compare to the modal experiment a data was taken on a frequency range of 100-5000 Hz. This did result in more noise in the data, especially at frequencies less than 500 Hz. An impedance measurement was made for each PZT by itself (Z_{xx}) and for each PZT simultaneously with PZT three (Z)

because it was the driving PZT for the modal analysis. This allows for the calculation of the transfer impedance, which can then be compared to the FRF's generated in the modal analysis. If it is assumed that the PZT sensors are identical the following formula describes the formulation of the transfer impedance (Z_{xy}) (Castanien and Liang 1996).

$$Z_{xy} = \frac{2ZZ_{xx}Z_{yy}}{-Z_{xx}Z_{yy} + Z(Z_{xx} + Z_{yy})} \tag{3.1}$$

An example of the impendence measurements and resulting transfer impedance for the joint at 40 ft-lbs is shown in figure 3.2.

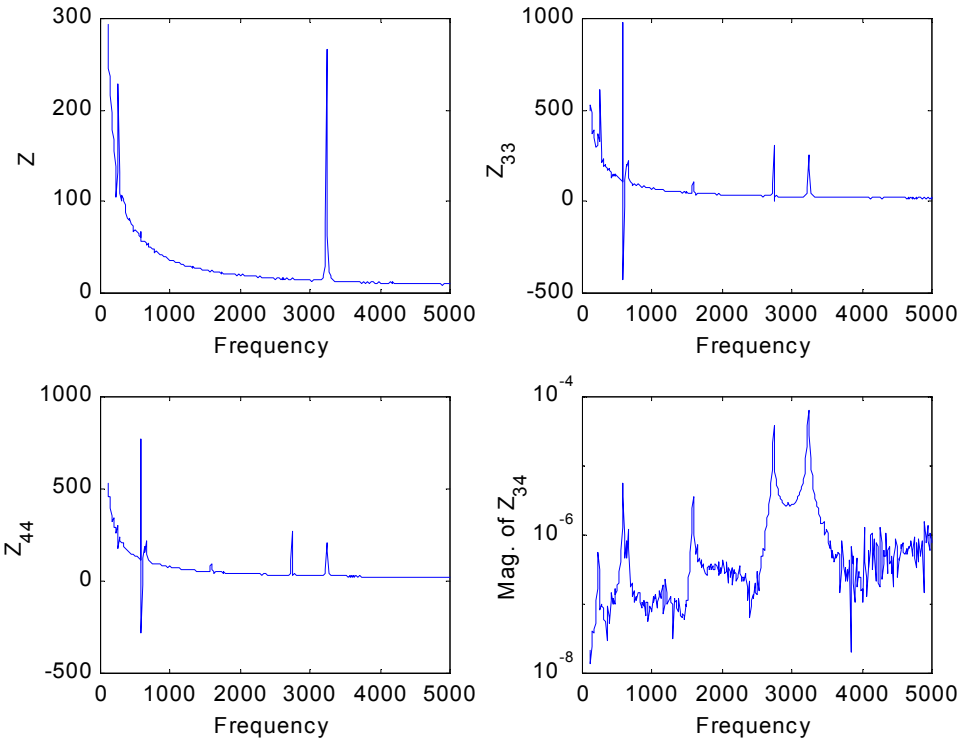

Figure 3.2 Example of impedance measurements and resulting transfer impedance

The FRF's from both the modal experiment and impedance experiment were analyzed using the rational fraction polynomial method. This method curve fits the data in the

frequency domain. Natural frequencies, damping ratios and residues, which can be used to generate mode shapes, were found for each torque level. Eight modes were fit in the using the modal data while only 5 were fit in the transfer impedance data. This is a result of some of the less prominent modes being hidden the increased amount of noise in the transfer impedance data. The results are summarized in Table 3.1 and 3.2. This confirms the closeness of the modal FRF data and transfer impedance data, which can also be seen in figure 3.3.

Table 3.1 Natural frequencies and damping ratio from analysis of modal data

40 ft-lbs		30 ft-lbs		20 ft-lbs		10 ft-lbs		hand-tight	
ωn (Hz)	damping	ωn (Hz)	damping	ωn (Hz)	damping	ωn (Hz)	damping	ωn (Hz)	damping
227.7	9.10E-03	225.7	6.00E-03	226.3	5.20E-03	226.5	4.30E-03	214.5	8.00E-03
580.3	3.30E-03	578.8	3.20E-03	579.1	9.30E-04	578.2	1.90E-03	564.3	3.10E-03
1573	1.80E-03	1565	1.60E-03	1557	1.70E-03	1524	1.80E-03	1487	4.70E-03
2731	1.30E-03	2719	1.80E-03	2673	2.00E-03	2547	1.40E-03	2102	1.80E-03
3237	2.00E-03	3220	2.30E-03	3208	2.30E-03	3185	2.40E-03	2874	3.00E-03
3702	7.00E-04	3689	7.50E-04	3685	7.30E-04	3663	7.60E-04	3397	9.60E-04
4221	1.70E-03	4202	1.90E-03	4190	1.90E-03	4141	2.00E-03	3922	3.00E-03
4259	6.90E-04	4252	5.30E-04	4248	7.70E-04	4236	7.20E-04	4083	2.50E-03

Table 3.2 Natural frequencies and damping ratio from analysis of impedance data

40 ft-lbs		30 ft-lbs		20 ft-lbs		10 ft-lbs		hand-tight	
ωn (Hz)	damping	ωn (Hz)	damping	ωn (Hz)	damping	ωn (Hz)	damping	ωn (Hz)	damping
226.5	3.50E-03	226.5	3.80E-03	226.9	6.20E-03	224.5	4.00E-03	213.4	9.10E-03
582.4	3.20E-06	581.5	3.90E-08	580.9	2.20E-05	579.5	7.10E-07	562.9	1.40E-07
1577	2.60E-06	1572	1.30E-06	1567	1.50E-03	1530	4.80E-08	1172	5.50E-07
2726	1.10E-05	2713	1.70E-03	2678	2.20E-04	2540	6.30E-04	2104	7.20E-07
3231	6.00E-06	3222	2.50E-06	3208	4.10E-07	3177	6.30E-04	2865	5.60E-03

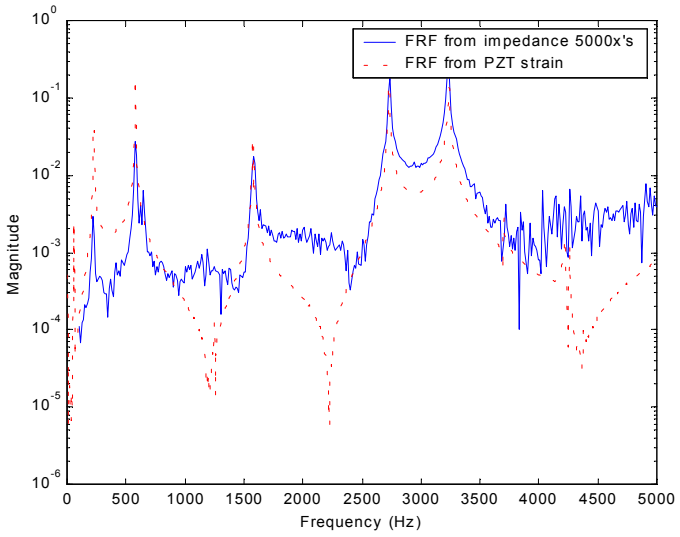

Figure 3.3 Impedance based and modal based response of joint at 40 ft-lbs

3.3.3 Results

Plots of the change in a mode's natural frequency versus torque level confirm that the two analyses again give approximately the same results. Furthermore, this indicates that the condition of a joint can be quantitatively monitored by looking at the variations in a resonant peak. If a resonant frequency goes down to certain level, then SMA actuators, similar to those describe in the next section, will be activated. Also, since each resonant peak does not change the same percentage as is the case with a change due to temperature (Park et al. 2000), by looking at more that one peak, false indications of damage due to change in temperature can be avoided. For example, if the resonant peak just above 2700 Hz for the 40 ft-lbs data shifted 3 percent and the resonant peak at approximately 1575 Hz for the 40 ft-lbs data shifted 3 percent that would indicate that the shifting peaks were due to a change in temperature. However, if the resonant peak just above 2700 Hz changed 7 percent and the resonant peak at 1575 Hz changed 3 percent, it would indicate that repair may be necessary.

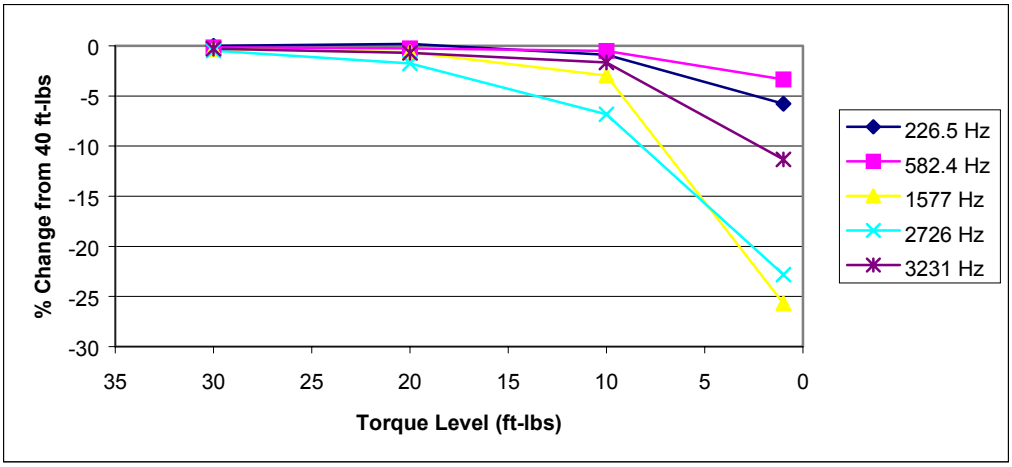

Figure 3.4 Natural frequency variation of modal data with torque level

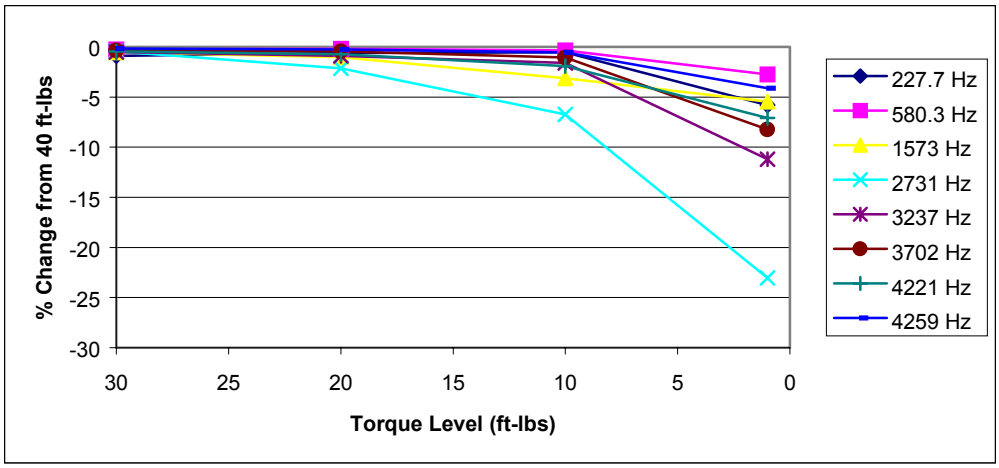

Figure 3.5 Natural frequency variation of transfer impedance data with torque level

3.4 Characterization of Damping

This section presents an investigation into friction damping and vibrations of beams with bolted lap joints. Two geometrically identical specimens with different characteristics are considered. The specimens are shown schematically in figure 3.6. The first specimen is a built-up beam. It consists of two long beam segments joined at the center by symmetric

plates. The plates connect to the beams in a lap joint configuration, fastened with a bolt. The second specimen has geometry identical to the first, but it is a monolithic structure machined from a single piece of steel.

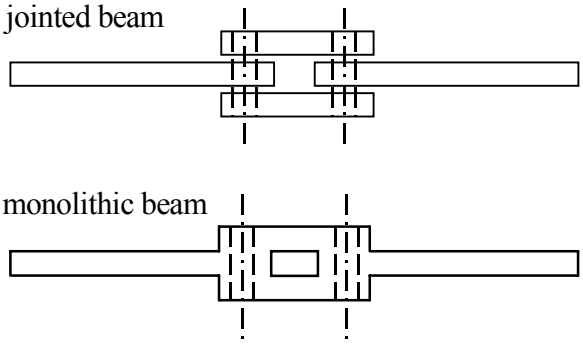

Figure 3.6 Schematics of beam specimens

The two experimental specimens exhibit substantially different dynamic behavior. While their modal frequencies are very close, their damping behaviors are very different. During vibration the jointed beam system assumes shapes like that shown in figure 3.7. At the interface between each beam segment and the plates that support it, longitudinal stress in the beam is great and longitudinal stress in the plates that form the joint is near zero. In view of this slippage (sometimes too small to measure accurately) occurs. Because the surface of any real structure element is rough, to some extent, energy dissipation occurs. This experiment and analysis attempts to characterize and model the effects of this energy dissipation.

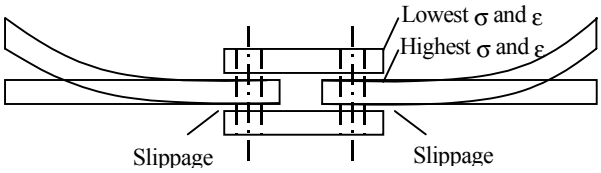

Figure 3.7 Jointed beam schematic

3.4.1 Experimental Configuration

The two test structures shown in figure 3.5 were evaluated in the experiment. The first structure consisted of two ten inch long steel beams connected by a lap joint. Dimensions

are provided in figure 3.8. The beam thickness and width are ¼ inch and 1.0 inch respectively. Two ¼ inch steel bolts with washers were used to sandwich the ends of the ten inch beams between two 3 ¼ inch long plates of steel. The bolts were tightened to 85 in-lbs. A ½ inch space was left between the ends of the 10" beams.

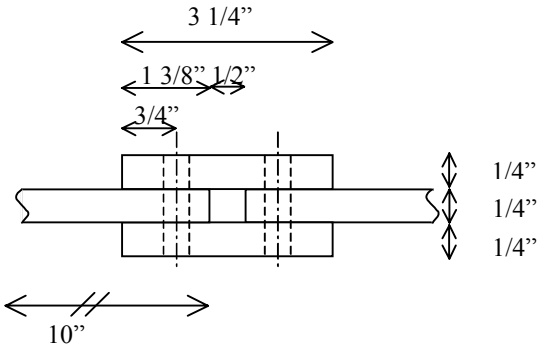

Figure 3.8 Segmented beam geometry

The second structure is an approximate geometric replica of the jointed beam machined from a single piece of steel. It is used as an experimental control. A schematic is shown in figure 3.9. Bolts were tightened through the holes in the structure as was done on the jointed beam. This was not required structurally in the solid beam, but to maintain similarity of the geometry and mass of the two beams.

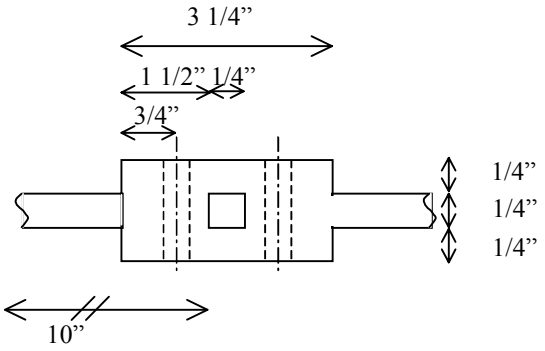

Figure 3.9 Solid beam geometry

During testing the beams were suspended from two approximately 3 ft. long sections of medical tubing in order to simulate a free-free boundary condition. The beams were

supported approximately 2 inches from each end. The beams were suspended so that the flexible plane of vibrations was oriented horizontally.

The beams were instrumented with one Endevco Isotron® 2250A-10 accelerometer fixed with wax to the beam, outside the joint near the center (figure 3.10). The accelerometer sensitivity and range were 10.01 mV/g and +/- 500 g respectively. A PCB impact hammer with a white plastic tip was used to excite the beams at various levels. Impacts were applied on the beam center axis, one inch from the end. The force transducer on the hammer (PCB 086C03) has a range of 0-500 lbf. and sensitivity of 10 mV/lbf.

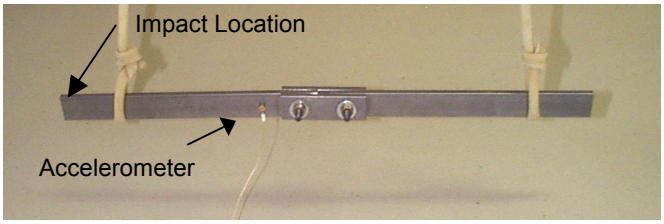

Figure 3.10 Beam instrumentation

Force and acceleration data were collected through the Data Physics Corporation ACE DP104 FFT Analyzer two-channel data acquisition system using SignalCalc ACE Dynamic Signal Analyzer software on a laptop computer running Microsoft Windows98. Data were recorded for 4.096 s at a rate of 2000 samples/s. This indicates a Nyquist frequency of 1000 Hz. The data were lowpass filtered (for anti-aliasing) at 781 Hz. The AC filter was set to 5 Hz. The data acquisition system was triggered when the hammer force surpassed 5 lbf. A 20 sample buffer was included at the beginning of each run. Twenty runs were averaged to estimate the beam frequency response functions. However, each time response was saved individually. The time histories were exported as ASCII text files to be analyzed in MATLAB. Figure 3.11 shows estimated frequency response functions for the beams.

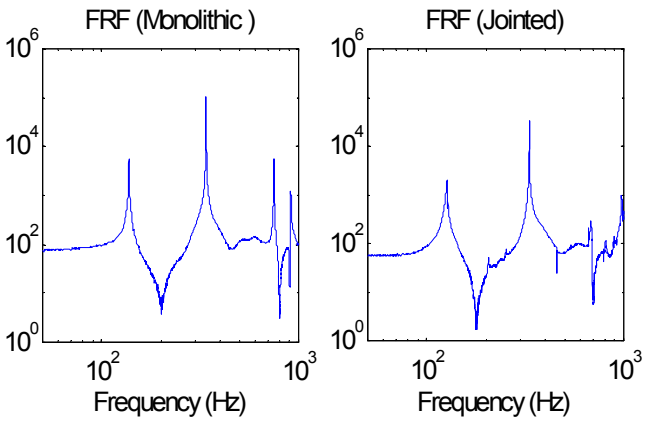

Figure 3.11 Sample frequency response functions of jointed and solid beams

Though substantial differences in some measures of behavior were anticipated, there are some clearly noticeable similarities. Specifically, the modal frequencies of the two experimental specimens are close. The first three modal frequencies of the jointed beam are 125, 326, and 689 Hz. The first three modal frequencies of the monolithic beam are 137, 339 and 750 Hz. This indicates that the two structures have very similar mass and stiffness characteristics. It is shown later that this similarity does not extend to the dissipative characteristics of the beams.

3.4.2 Analysis of Experimental Data

Two approaches are used in this investigation to characterize energy dissipation in the beam systems under consideration. First, linear models are used to describe energy dissipation realized in the experimental systems. Later, linear and nonlinear models are used to describe energy dissipation in mathematical models of the physical systems.

Two linear frameworks are used to characterize the beams' experimental behavior realized in the laboratory. These are the log decrement and half power bandwidth frameworks. The log decrement approach is implemented in a local linear construct to approximate energy dissipation in both beams. This is the primary approach to experimental characterization of the beams.

To apply the log decrement approach, the beam was excited as described in the previous section. When the excitation was no longer active, the free decay of the beam was observed. From a separate analysis, the modal frequencies of each beam were assessed. Then each oscillatory decaying acceleration signal was low pass filtered between the first and second oscillatory modes to eliminate higher mode contributions. (Note that two very low frequency rigid body-type modes associated with motion of the beam on its very soft elastic supports did not appear in the data because, as mentioned previously, the measured data were high pass filtered at about 5 Hz.)

To establish the system decay characteristics accurately, the analytic function of the Hilbert transform was computed for each filtered oscillatory signal. This function is an approximate envelope of the signal. In all cases it forms a decaying, approximately exponential curve.

An analysis program divides the decay curve into ten segments that overlap 50 percent. It retains data whose amplitudes are greater than 10 percent of the peak amplitude. The program estimates the average amplitude of the data in each segment. It then takes the natural logarithm of each data segment and fits a straight line to the data using a least squares approach. The system damping factor in the first oscillatory mode is inferred from the parameters of the straight line. The damping factor in each segment is associated with the average amplitude of motion during that segment. Damping versus amplitude is plotted using measurements from several tests.

The plots described above supply a visual means for determining system linearity. When the estimates of damping factor plotted as a function of amplitude form a horizontal line, the system mode can be inferred to be linear with damping factor that is constant over all response amplitudes. When the estimates of damping factor plotted as a function of amplitude form a curve with variable ordinate, then the damping coefficient is a nonlinear function of amplitude. When such a curve appears to have a simple form it may be possible to approximate the amplitude dependence of damping factor on displacement or velocity

amplitude. The manner in which the damping factors were established implies that these experimental systems can be treated as locally linear.

The half power bandwidth estimate uses MATLAB's Transfer Function Estimate (TFE) program to determine the system's frequency response function (FRF). It takes multiple measured acceleration vectors, windows them, and concatenates them to create one continuous vector. Except for windowing, the same is done for the impulsive forces. The excitation and response vectors are inputs to the TFE program. The resulting FRF is input to a modal frequency approximation program, which records the modal frequencies and the corresponding magnitudes of the FRF. The first mode is used for the half power bandwidth analysis. The damping coefficient is estimated in the usual manner. This approach is only used to check the results of the log decrement analysis.

3.4.3 Mathematical Model

Simple finite element models of the jointed and monolithic beams were created. The FE models use the structural dynamic framework of the simultaneous ordinary differential equation given by

$$[m]\{\ddot{x}\}+\{R(x,\dot{x})\}=\{q\} \tag{3.2}$$

where x is displacement at the system degrees of freedom, the dots over denote differentiation with respect to time, $[m]$ is the mass matrix, $\{R\}$ is the vector of nonlinear restoring force functions (dependent on displacement and velocity), and $\{q\}$ is the forcing function vector. Initial conditions must be specified to solve the equation of motion.

The monolithic beam was modeled in the linear framework. The restoring force governing the system is

$$\{R(x,\dot{x})\}=[c]\{\dot{x}\}+[k]\{x\} \tag{3.3}$$

where [c] and [k] are the viscous damping and stiffness matrices.

The operations of the FE code include synthesis of the mass and stiffness matrices, eigenvalue analysis (for linear problems), and solution of the system of ordinary differential equations. The code is implemented in MATLAB. Beam elements with two degrees of freedom (rotational and translational) are used to construct the stiffness and mass matrices. The mass matrix is diagonal. The built in eigenvalue analysis (eig) is used to solve the eigenvalue problem. The results are presented later.

Jointed beam analysis requires the capability to solve nonlinear ordinary differential equations. The nonlinear behavior is approximated by simplifying equation 3.2 by constraining system motion to a single linear mode. Specifically, the vector displacement and velocity responses of the system were approximated using

$$\{x(t)\} \cong \xi_k(t)\{\phi_k\}, \{\dot{x}(t)\} \cong \dot{\xi}_k(t)\{\phi_k\} \tag{3.4}$$

where $\xi_k(t)$ is displacement in the kth modal coordinate, $\xi_{\cdot k}(t)$ is the corresponding velocity and φ_k is the kth orthanormal mode shape. It is recognized that this approximation can never converge to the exact solution. However, experimental observations indicate that this is a relatively accurate approximation. Thus the restoring force for the nonlinear system is modeled as

$$\{R(x,\dot{x})\} = [c]\{\dot{x}\} + [k]\{x\} + \{R_{nl}(x,\dot{x})\} \tag{3.5}$$

General system damping is modeled as viscous. $\{R_{nl}(x,\dot{x})\}$ is zero except where degrees of freedom are attached with nonlinear elements.

Figure 3.12 shows a schematic of part of the FE model. Beam elements are shown as blocks. The nonlinear connections are included in $\{R_{nl}(x,\dot{x})\}$.

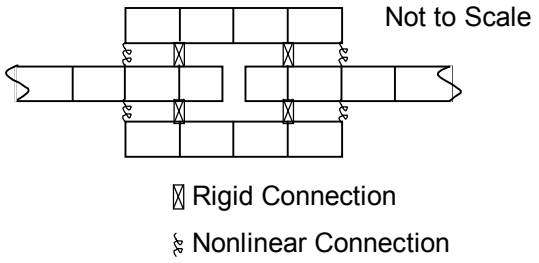

Figure 3.12 Nonlinear finite element model schematic

Friction is modeled using a form of the bristles construct often referred to as the Lu-Gre model (see Gaul and Nitche 2001; Haessing and Friedland, 1991). The assumptions underlying the model follow. Opposing frictional surfaces are irregular and the irregularities can be modeled with bristles. When opposing surfaces move relative to one another some bristles establish and/or maintain contact while others lose contact. The bristles in contact and this results in a displacement related motion resistance. Based on experimental evidence, it is assumed that the fraction of bristles in contact is a function of velocity. Based on these assumptions the restoring force, opposing motion at the frictional joint is

$$R = \alpha N k \left| \Delta x \right| \tag{3.6}$$

where α = average fraction of bristles in contact, N = number of bristles, k = bristle stiffness, Δx = change in displacement over time interval of interest. For this investigation α was given the form

$$\alpha = \gamma_0 e^{-v^2/2\beta^2} + \gamma_1 \tag{3.7}$$

where β, γ_0, and γ_1 are parameters of the model.

Experimental results (summarized in the following section) showed that the Bristle model incorrectly predicts the qualitative behavior of the lap-jointed beam. The model can be modified by inserting explicit dependence on velocity. When this is done, energy

dissipation in the mathematical model of the beam can be made to match the experimental results. The model developed is

$$R = v^{\frac{1}{4}} \alpha N k |\Delta x| \tag{3.8}$$

This restoring force equals zero at zero velocity.

3.4.4 Experimental Results

The experiments described in a previous section were performed and system excitations and responses were measured. Two measured acceleration response time histories are shown in figures 3.13 and 3.14. The first is the low pass filtered acceleration response of the jointed beam with filter cutoff frequency of 240 Hz. The second is the low pass filtered acceleration response of the monolithic beam with filter cutoff frequency of 240 Hz. Below each time history is the envelope formed by the analytic function of the Hilbert transform of the response time history. Though not apparent from the time histories, the fundamental frequency of response of the jointed beam is 125 Hz, and that of the monolithic beam is 137 Hz. It is clear from the graphs that the average decay rates of the jointed and monolithic beams differ greatly.

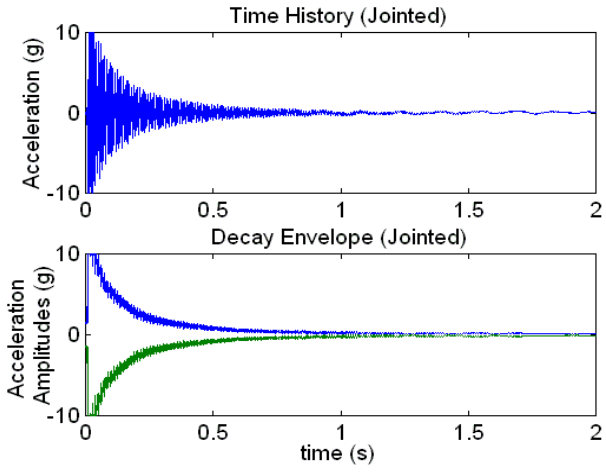

Figure 3.13 Typical response time history and its envelope for the jointed beam

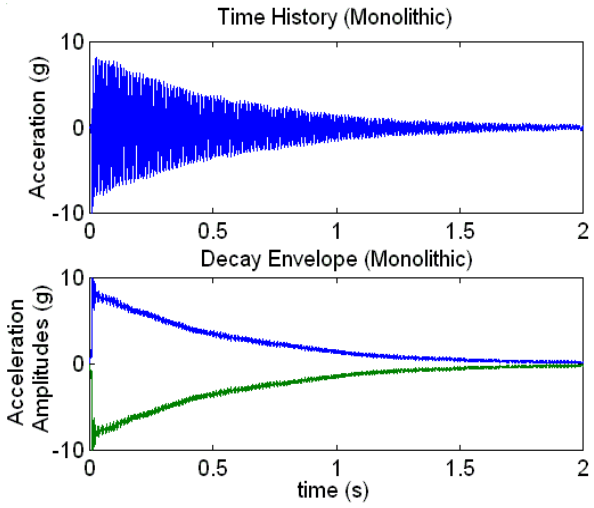

Figure 3.14 Typical response time history and its envelope for the monolithic beam

The amplitude decay signals were analyzed as specified in the Analysis of Experimental Data Section. Local linear estimates of damping factors were computed for both beams and are shown in figures 3.15 and 3.16. Both figures depict local linear estimates of damping factors as a function of velocity amplitude. The former presents this information for the monolithic beam; the latter for the jointed beam. Each figure presents the results of 20 tests. The data are scattered because (1) the measurements include random noise, and (2) the system, environment, and boundary conditions vary slightly from one test to the next.

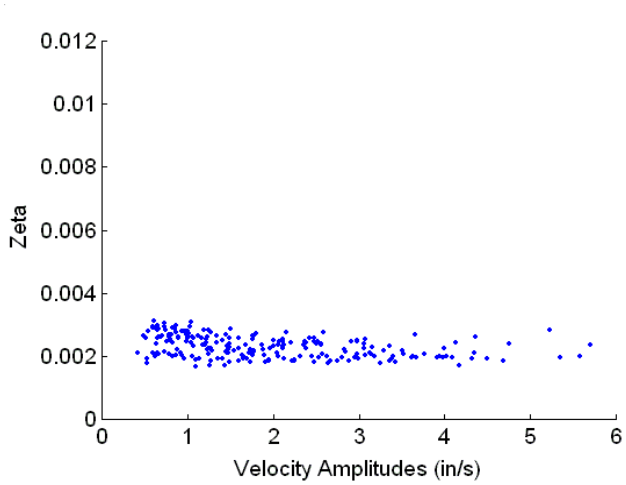

Figure 3.15. Estimates of local linear damping factor for the monolithic beam

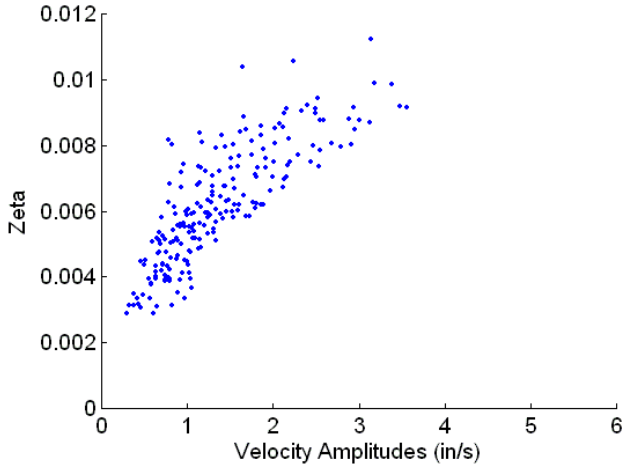

Figure 3.16 Estimates of local linear damping factor for the jointed beam

The data in figure 3.15 indicate that damping level is constant with respect to amplitude, for the monolithic beam, over the range of amplitudes considered in these experiments. The sample mean of the damping factor estimates in figure 3.15 is 0.22 percent.

In contrast, the data in figure 3.16 show that damping increases with velocity amplitude in the jointed beam. Over the range of amplitudes considered in those experiments local linear damping factor estimates vary from about 0.3 percent at an amplitude of 0.5 in/s to about one percent at an amplitude of 3.5 in/s. It is clear that the slope of the mean of the damping factors diminishes with increasing velocity amplitude. This is to be expected because (1) damping effects cannot increase without bound, and (2) the physical phenomenon may restrict damping effects to some upper limit.

The average damping factor of the two systems was estimated using the half power bandwidth approach. The damping factor of the monolithic beam was estimated to be 0.24 percent, and that of the jointed beam was estimated to be 0.64 percent. These values tend to confirm the results shown in figures 3.15 and 3.16, because they represent averages formed using responses at all levels.

3.4.5 Analytical Results

The linear and nonlinear analyses described in the Mathematical Model Section were performed with the objective of simulating the behavior of the two experimental systems. Both linear and nonlinear analyses are modal-based. The response in a single mode is considered. This modal analysis is exact for the linear system, but only an approximation for the nonlinear system.

Modal frequencies for the linear system were estimated as 134, 333, and 730 Hz (versus 137, 339, and 750 Hz, for the monolithic experimental system). The modal analysis that forms the basis for analysis of the nonlinear beam yielded modal frequencies of 116, 339, and 624 Hz (versus 125, 326, and 689 for the jointed experimental system). The reason for the differences between the analyzed modal frequencies and those experimentally obtained is primarily the imperfection of the mathematical models. The form of the friction model is given in Eq. (5). The parameters used in this investigation are: $\beta = 0.2$, $X = 0.3$, $\gamma_1 = 0.7$ and $Nk = 2.5 \times 10^9$.

The analyzed velocity response time histories of the linear and nonlinear beams in their first oscillatory modes are shown in Figures 3.17 and 3.18, along with their envelopes as represented by the analytic function of the Hilbert transform. (Velocity is shown because only displacement and velocity are computed.)

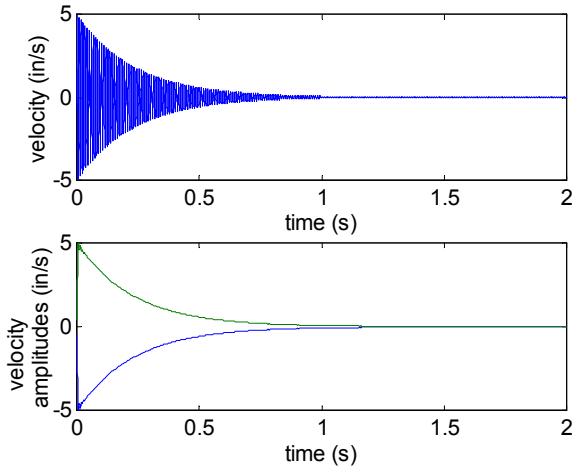

Figure 3.17 Computed velocity response of linear system, and its envelope

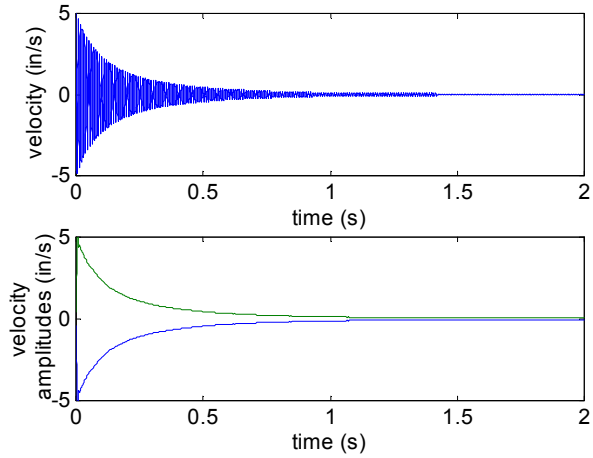

Figure 3.18 Computed velocity response of nonlinear system, and its envelope

The analyzed time histories clearly mimic the experimental measurements. The simulated motion in the jointed beam decays more rapidly than the corresponding motion in the monolithic beam. Further, the frequencies of motion accurately duplicate the fundamental frequencies of the experimental beams, but this should be expected because the modal approximation forces motion to occur at a particular frequency.

As for the experimental data, local linear damping factor estimates from the analyzed responses were computed. The results are shown in figures 3.19 and 3.20.

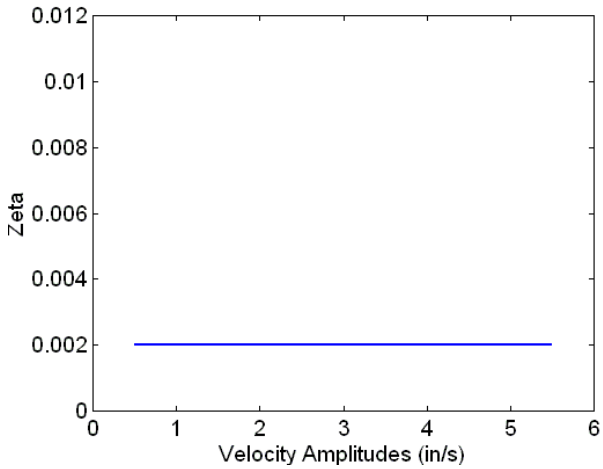

Figure 3.19 Estimates of local linear damping factor for the linear beam model

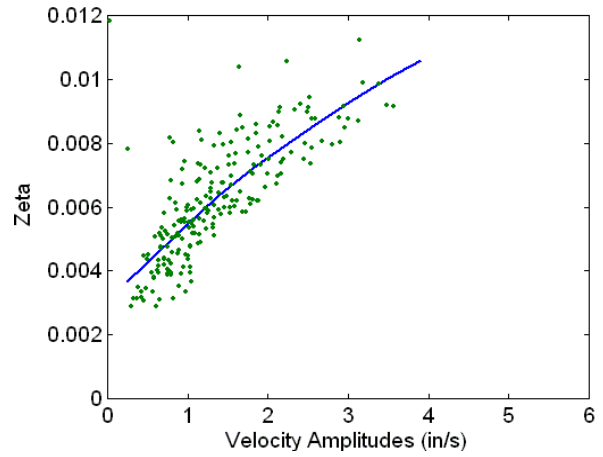

Figure 3.20 Estimates of local linear damping factor for the nonlinear beam model (experimental data shown for reference)

Figure 3.19 shows that damping in the linear model is a constant. This is appropriate because it is constrained to be so.

Figure 3.20 shows that the local linear damping factor in the nonlinear beam model is variable and resembles the mean of the experimental data obtained from experiments on the jointed beam. This shows that the mathematical model for friction given by equation 3.8 plausibly explains energy dissipation in the jointed beam. Though figure 3.19

demonstrates the plausibility of the modified Bristle model, much more experimentation and analysis are required to demonstrate its optimality.

3.5 Conclusions

A bolted joint was monitored upon loosening with a traditional modal method and transfer impedance method. The transfer impedance method has given results very similar to that of the modal method. Therefore it is possible to use impedance to monitor changes in resonant peaks to quantify torque changes as damage to joints. Higher frequencies are a generally a better indicator of damage because the change in frequency at low frequency ranges is very small, even though the percentage change may be slightly larger.

Experiments were performed on two simple geometrically identical beams in an attempt to characterize the nonlinear lap joint behavior. The beams were impact tested and response decay characteristics were used to infer modal damping. The experimental results were cast as local linear damping factor versus velocity amplitude. A monolithic beam displayed constant damping behavior. A lap jointed beam displayed damping that is an increasing function of amplitude of vibration. This could potentially be incorporated into the impedance method to rule out forms of damage to the structure other than the loosening of the joint where activation of the self-healing mechanism would not be appropriate. The model could also be useful in predicting the response when using various levels of excitation that are possible when using FFT analyzers for the low-cost method of making impedance measurements.

Approximate analyses were performed to test the plausibility of a model for joint friction. Both linear and approximate nonlinear finite element models for beam behavior were developed. The modal frequencies of the linear model matched the corresponding values for the monolithic system closely. The approximate nonlinear analysis was used to

develop the relation between local linear damping factor and velocity amplitude. The analytical results matched the experimental results closely. This demonstrates the plausibility of the Bristle model.

Though the Bristle construct appears to offer a plausible, phenomenological alternative for modeling joint friction, it is recommended that further study be conducted prior to adoption in specific applications. In addition, physical systems and their mathematical models should be exercised and validated using other methods and forms of excitation.

A unified automatic process should be developed to evaluate when a joint has damage requiring action. This should include all of the issues investigated here as well as those evaluated by various other researchers including temperature and other environmental effects, other damage modes and quantitative assessment methods.